# Interface and Electrode Microstructure Engineering for Optimizing Performance of the LiNiO$_2$ Cathode in All-Solid-State Batteries

Yuan Ma,* Ruizhuo Zhang, Yanjiao Ma, Thomas Diemant, Yushu Tang, Seyedhosein Payandeh, Damian Goonetilleke, David Kitsche, Xu Liu, Jing Lin, Aleksandr Kondrakov, and Torsten Brezesinski*

ABSTRACT: Solid-state batteries (SSBs) utilizing superionic thiophosphate solid electrolytes (SEs), such as argyrodite Li$_6$PS$_5$Cl, are attracting great interest as a potential solution for safe, high-energy-density electrochemical energy storage. However, the development of high-capacity cathodes remains a major challenge. Herein, we present an effective design strategy to improve the cyclability of the layered Co-free oxide cathode active material (CAM) LiNiO$_2$, consisting of surface modification and electrode microstructure engineering. After optimization, the SSB cells were found to deliver high capacities ($q_{dis} \approx 200$ mAh/g$_{CAM}$) and to cycle stably for hundreds of hours. A combination of operando and ex situ characterization techniques was employed to reveal the mechanism of optimization in overcoming several issues of LiNiO$_2$, including poor SE compatibility, outgassing, and state-of-charge heterogeneity. Tailoring the microstructure of the composite cathode and increasing the CAM|SE interface stability enable superior electrochemical performance.
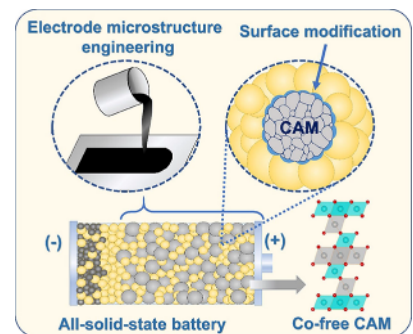
INTRODUCTION

Solid-state batteries (SSBs) are considered promising contenders for next-generation energy-storage systems.[1,2] This technology promises to eliminate safety concerns by replacing the flammable liquid in conventional Li-ion batteries (LIBs) with superionic inorganic solid electrolytes (SEs).[1,3] Inorganic SEs offer mechanical rigidity and exhibit a high lithium transference number, thus enabling the use of high-capacity anodes, such as Li metal or Si.[4,5] However, further development of SSBs is required to replicate the performance of the state-of-the-art LIB technology.[6]

The implementation of high-performance cathodes into SSBs is the primary factor.[7] Unlike conventional LIBs, it is necessary to fabricate a composite by mixing SE with a cathode active material (CAM) and to ensure sufficient contact between the two components. Especially electrode microstructure engineering is crucial for constructing highly percolated ionic/electronic transport pathways (preventing local agglomeration of CAM and SE particles, etc.).[8,9] Layered Ni-rich oxide CAMs [LiNi$_{1-x-y}$Co$_x$Mn$_y$O$_2$ (NCM or NMC)] and thiophosphate SEs hold promise for application at the positive electrode side due to high theoretical specific capacity ($q_{th} = 275$ mAh/g) and superior ionic conductivity ($\sigma_{ion,rt} \geq 2$ mS/cm for Li$_6$PS$_5$Cl and related materials).[10,11] However, thiophosphate SEs possess a narrow electrochemical stability window and show poor compatibility with oxide cathodes, ultimately resulting in unfavorable side reactions at the CAM| SE interface and impedance buildup during cycling (by impeding charge transfer and transport).[1,12] Aside from that,

mechanical degradation and electronic/ionic contact loss caused by volume changes ("breathing"), as well as unfavorable outgassing, inhibit the performance of Ni-rich CAMs in SSBs.[13,14]

In the present work, we report on performance optimization of a prototype cathode consisting of LiNiO$_2$ and argyrodite Li$_6$PS$_5$Cl as the CAM and SE, respectively. The understanding of charge storage in LiNiO$_2$ (including the major limiting factors) is of great academic and industrial interest. LIBs and SSBs using LiNiO$_2$, which is isostructural with NCM and other Ni-rich cathodes, offer a high energy density but are limited in their cycling stability.[15–17] Li$_6$PS$_5$Cl, on the other hand, exhibits a low Young's modulus, in addition to a high Li-ion conductivity, ensuring proper mechanical integrity.[11,18] The system was optimized first using surface modification by coating the CAM in order to stabilize the interface with the SE. Further optimization was accomplished by transitioning from pelletized to a slurry/tape-cast cathode with the objective to improve the dispersion of CAM particles in the SE matrix. Notably, the manufactured composite cathode shows good cycling performance in high-loading SSB cells. The combination of operando and complementary ex situ characterization
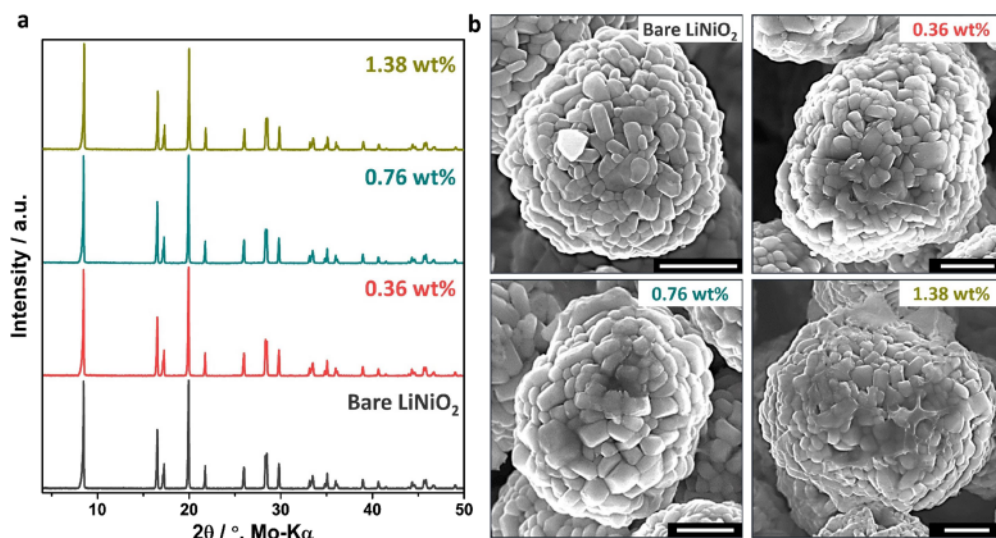
Figure 1. (a) Powder XRD patterns of the bare and coated $LiNiO_2$ CAMs and (b) corresponding SEM images of the secondary particles (scale bar: 2 μm).
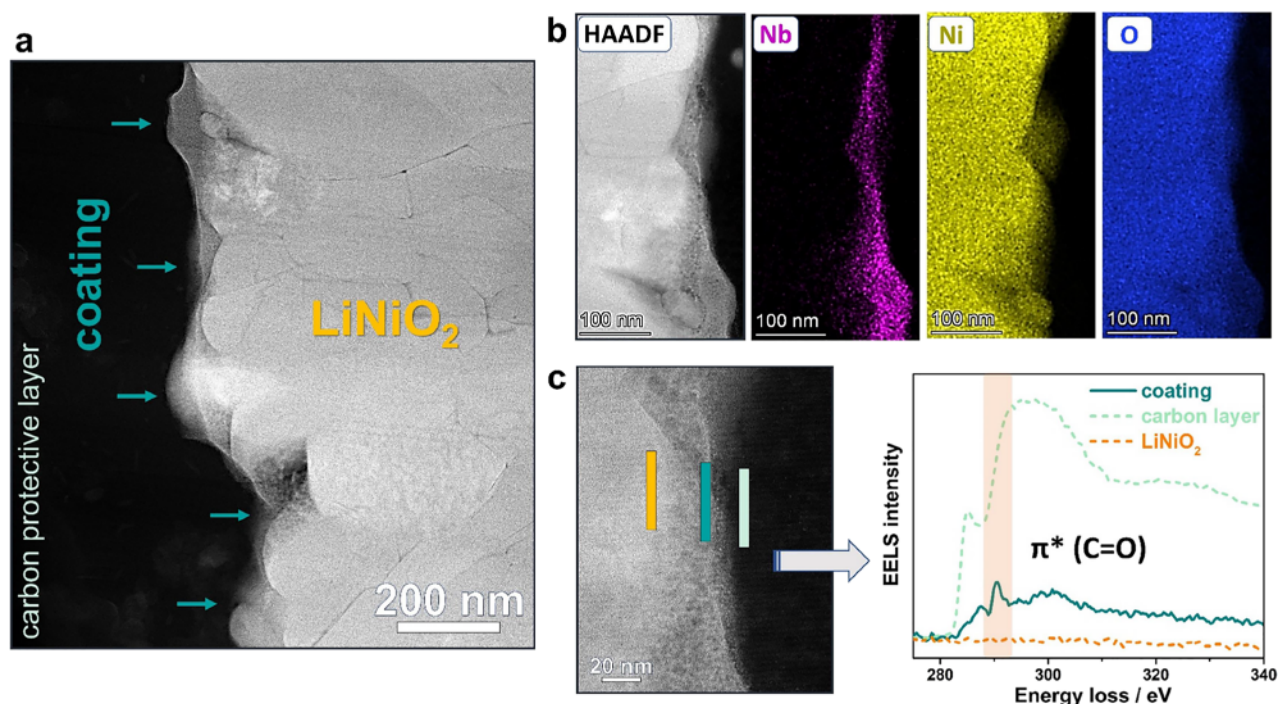

Figure 2. Surface structure of the 0.76 wt % coated $LiNiO_2$ CAM. (a) HAADF STEM image and (b) EDS maps of a secondary particle cross section. (c) EEL spectra collected from the areas indicated in the respective STEM image.

techniques revealed the underlying working mechanism/principle of the protective coating and the origin of the differences in cyclability between pelletized and slurry-cast electrodes.

RESULTS AND DISCUSSION

$LiNbO_3$ was used to coat the CAM surface, as it has been previously demonstrated as an effective material to reduce interfacial degradation and can be applied through a facile solution-based (sol−gel) process.[19,20] $LiNiO_2$ was synthesized by a classical solid-state reaction. Three CAMs with different $LiNbO_3$ contents of 0.36, 0.76, and 1.38 wt % were prepared (see inductively coupled plasma-optical emission spectroscopy

(ICP-OES) results in Table S1) to determine the optimal coating thickness. Figure 1 shows powder X-ray diffraction (XRD) patterns and scanning electron microscopy (SEM) images collected from bare and coated CAMs. Figures 1a and S1−S4 confirm that all of them have the expected O3-type layered structure ($R−3m$ space group). Although the weight content of the coating is too low for analysis by XRD, Rietveld refinement (see Table S2) indicated that the structural parameters (lattice parameters, unit-cell volume, and degree of cation intermixing) do not differ much among the samples. This suggests that the coating process has a negligible effect on the bulk structure of $LiNiO_2$.[21] The microscopy images (Figure 1b) reveal the expected polycrystalline morphology of the
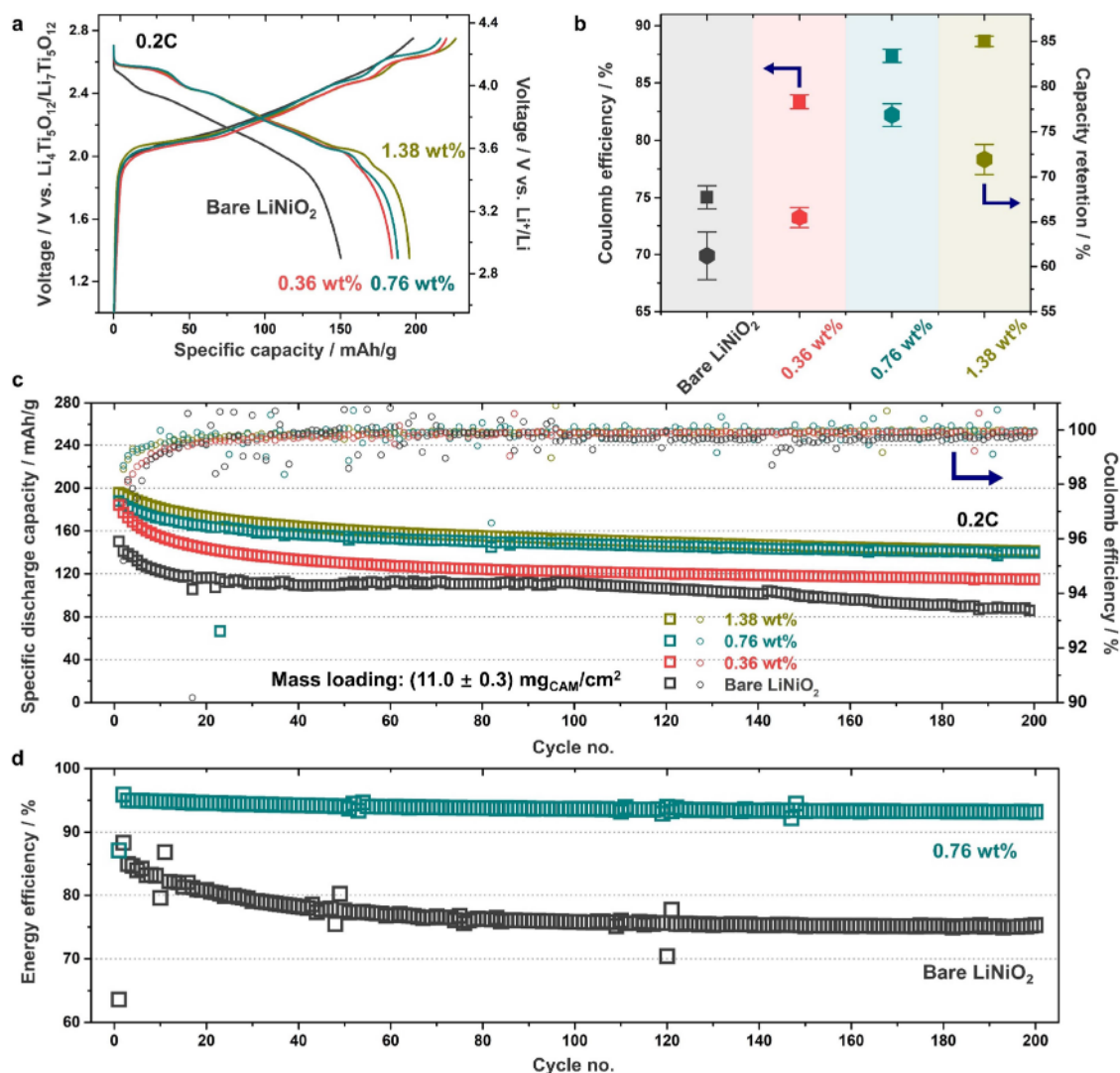
Figure 3. Cycling performance of the bare and coated $LiNiO_2$ CAMs in SSB cells. (a) First-cycle voltage profiles. (b) Initial Coulomb efficiency and capacity retention after 200 cycles at 45 °C and 0.2C rate. Error bars represent the standard deviation from three independent cells. (c) Specific discharge capacity and Coulomb efficiency vs the cycle number. (d) Energy efficiency of SSB cells using the bare and 0.76 wt % coated $LiNiO_2$.

samples, with a typical diameter of about 4 μm. The surface coating is also visible to some degree, especially for the 1.38 wt % coated CAM.

High-angle annular dark-field (HAADF) scanning transmission electron microscopy (STEM) and energy-dispersive X-ray spectroscopy (EDS) were used to better resolve the structure and composition of the coating (shown for the 0.76 wt % coated CAM in Figure 2). Measurements were conducted on cross-section lamella prepared by focused ion beam (FIB) machining. A carbon layer was deposited onto the particle surface to avoid damage to the coating during specimen preparation. As evident from Figure 2a,b, the $LiNbO_3$ appears as a distinct layer on the surface of the secondary particles with good coverage at least on the scale of the STEM/EDS characterization. The thickness of the coating ranges from about 10 to 50 nm. This variation in thickness is an inherent problem of the wet-coating technique but can likely be improved in the future by using physical deposition methods.[11,19,22,23] Figure 2c presents a high-magnification STEM image along with electron energy loss spectroscopy (EELS) data collected from different areas across the surface. From the image, the coating appears to have nanoparticulate

nature, which agrees with previous results from FIB-SEM measurements.[24] Comparison of the EEL (carbon K-edge) spectra uncovers the presence of carbonates, probably Li_2CO_3, as a second coating component.[25,26] Aside from that, high-resolution STEM imaging suggests some tendency toward niobium surface doping and further revealed the presence of rocksalt-like regions in the vicinity of the $LiNiO_2$|coating interface (see Figure S5).[27,28] As can be seen from the STEM image shown in Figure S6, the 0.36 wt % coated CAM exhibits an (isolated) island-type coating structure (relatively low surface coverage), whereas the 0.76 and 1.38 wt % coated samples share similar properties with regards to coating thickness and uniformity (see Figures 2a and S7). This apparent difference is also reflected in the electrochemical response.

To evaluate the influence of the coating on the electrochemical properties, composite cathodes with a high areal loading [(11.0 ± 0.3) mg_{CAM}/cm^2, ~2.5 mAh/cm^2] were incorporated into pelletized SSB full cells using Li_6PS_5Cl, $Li_4Ti_5O_{12}$, and Super C65 as the SE, anode active material, and conductive additive, respectively. The cells were cycled at 45 °C and 0.2C rate (with 1C = 225 mA/g_{CAM}) over 200 cycles in
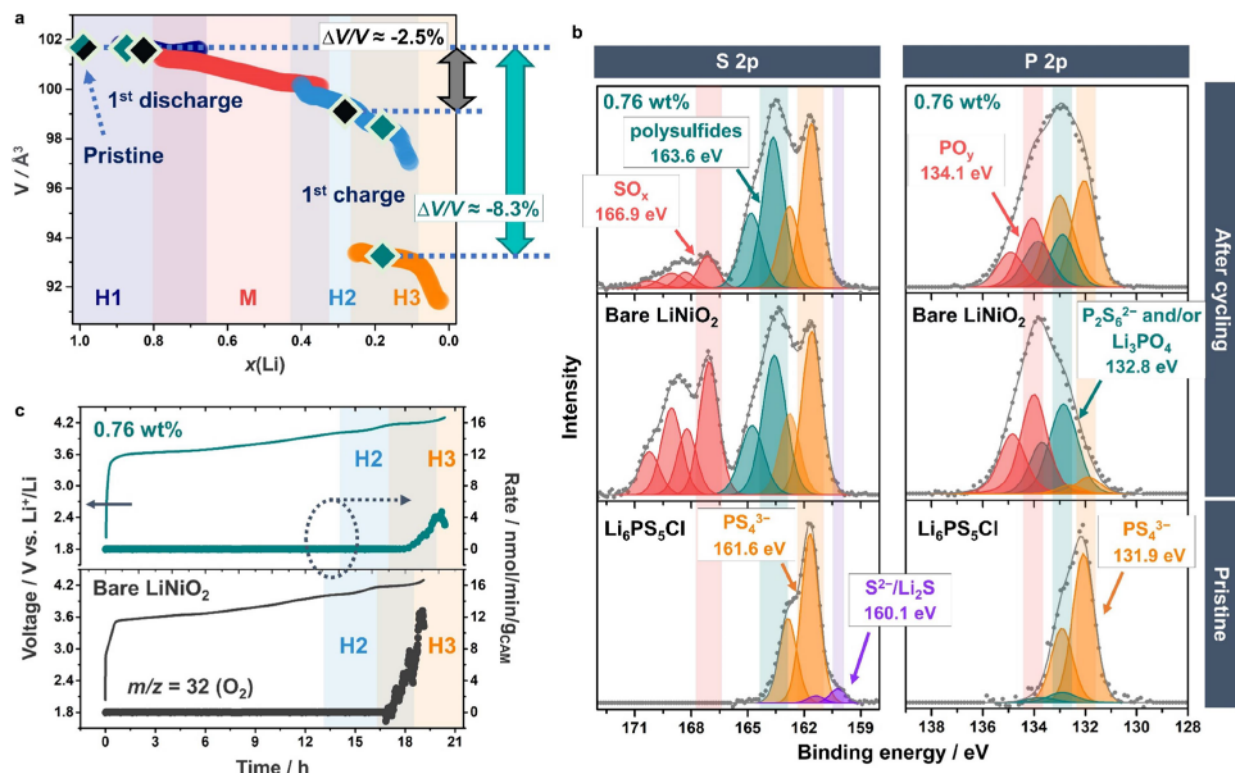
Figure 4. (a) Evolution of the unit-cell volume with lithium content determined by Rietveld analysis of operando XRD data collected during cycling of LiNiO$_2$ in a LIB reference half-cell. Structural parameters for the bare and 0.76 wt % coated LiNiO$_2$ CAMs from ex situ XRD are indicated by black and green diamonds, respectively. (b) Detailed XP spectra showing the S 2p and P 2p core-level regions for pristine Li$_6$PS$_5$Cl and the pelletized composite cathodes after 200 cycles at 45 °C and 0.2C rate. (c) In situ gas analysis of the SSB cells in the initial charge cycle at 45 °C and 0.05C rate.

a voltage window of 1.35−2.75 V vs Li$_4$Ti$_5$O$_{12}$/Li$_7$Ti$_5$O$_{12}$ (∼2.9−4.3 V vs Li$^+$/Li) and the respective electrochemical data are presented in Figure 3. The first-cycle charge/discharge curves (Figure 3a) reveal a significant improvement in performance after coating. In fact, the coated LiNiO$_2$ samples experienced much smaller voltage drops and consistently showed lower overpotentials than the bare counterpart due to reduced cathode interface resistance. As expected, they delivered greater specific capacities and showed improved Coulomb efficiencies (e.g., q_{dis} = 196 mAh/g and Φ_Q = 88% for the 1.38 wt % coated CAM in the initial cycle). They also demonstrated good long-term cycling performance, and, interestingly, the improvement to capacity retention suggests that there may be an optimal limit for the coating content: bare < 0.36 wt % < 1.38 wt % < 0.76 wt % (see Figure 3b,c). The relatively low surface coverage helps to explain the inferior cyclability of the 0.36 wt % coated CAM,[19,22] while the similar electrochemical response of the 0.76 and 1.38 wt % coated samples is likely due to the similarity in coating properties, as mentioned above.

In the following, the 0.76 wt % coated CAM will be examined in some more detail. Figure 3d compares the energy efficiency of cells with the bare and coated LiNiO$_2$. The energy efficiency is an important performance index but is often neglected in academia. It is defined as the ratio of energy released during discharge to the energy stored upon charge.[29,30] In contrast to the bare material, the energy efficiency stabilized above 90% when the coated LiNiO$_2$ was used, suggesting that the protective surface layer is capable of

mitigating energy loss by preventing adverse side reactions from occurring during battery operation.

To better understand the differences in cyclability, operando and ex situ/postmortem analyses were applied to bare and coated LiNiO$_2$, as summarized in Figure 4. The effect of mechanical degradation (particle fracture, contact loss, etc.) on performance is first discussed. This type of degradation mostly originates from the anisotropic volume variation in layered Ni-rich oxide CAMs.[31−34] To estimate the state-of-charge (SOC) achieved in the SSB cells, operando XRD data collected during cycling of bare LiNiO$_2$ in a LIB half-cell were used as a reference. The data are meant to provide the changes/trends in structural parameters as a function of lithium content, see Figure 4a (further details can be found elsewhere).[15] Note that the unit-cell volume versus lithium content curve can be divided into four regions, encompassing the structural characteristics of the hexagonal H1 (purple), monoclinic M (red), hexagonal H2 (blue), and hexagonal H3 (orange) phases. Since the coated material delivers a much higher specific capacity and achieves a greater degree of delithiation, this is accompanied by a more severe relative volume contraction ($\Delta V/V \approx -8.3\%$ at ∼4.3 V vs Li$^+$/Li), as indicated by the green diamonds in Figure 4a, due to collapse of the layered structure (H2−H3 phase transition) at high SOC. In contrast, the $\Delta V/V$ is determined to be about −2.5% for the bare counterpart (black diamonds), which does not achieve enough delithiation to experience the H2−H3 transition. This agrees well with the lack of the H2−H3 peak in the differential capacity curves shown in Figure S8. The (comparatively) low absolute relative volume contraction

found for the bare $LiNiO_2$ can be attributed to unwanted side reactions occurring during the initial charge, which result in a loss of lithium inventory of the cell and impedance buildup. Despite the significant difference in volume variation, the comparison indicates that the primary reason for performance degradation is not due to mechanical separation between CAM and SE. In addition, the use of a CAM with a small particle size helps to maintain good contact with the SE.[13,20,35] This conclusion is in line with the cycling behavior of the cells, meaning there is no sudden drop in capacity after the initial cycles regardless of using the bare or coated $LiNiO_2$.[36]

In recent years, the limited stability of the cathode (CAM| SE) interface has been shown to cause performance impairments.[1] To examine the potentially adverse effects of interfacial side reactions on cycling performance, X-ray photoelectron spectroscopy (XPS) measurements were conducted on the pristine SE and the pelletized cathodes after 200 cycles at 45 °C and 0.2C rate. We limit our discussion to the S 2p and P 2p core levels (see Figure 4b), which typically reflect the most significant changes due to, among others, electrochemical oxidation. The respective spectra of Li_6PS_5Cl show several doublets, in agreement with previous results.[13,37] The major doublet in the S 2p (S $2p_{3/2}$ at 161.6 eV) and P 2p regions (P $2p_{3/2}$ at 131.9 eV) can be attributed to the PS_4^{3-} units of the argyrodite structure.[24] The data also indicate the presence of free S^{2-}/Li_2S (S $2p_{3/2}$ at 160.1 eV) and some other minor impurities, such as $P_2S_6^{2-}$ and/or Li_3PO_4 (P $2p_{3/2}$ at 132.8 eV).[13,38−40] After cycling, new doublets at higher binding energies appear in the S 2p spectra due to chemical and electrochemical SE degradation. These can be assigned to polysulfides (S $2p_{3/2}$ at 163.6 eV) and SO_x species (S $2p_{3/2}$ beyond 165 eV).[11,35,41] The formation of oxygenated sulfur-based decomposition products is directly related to the side reactions at the CAM|SE interface since $LiNiO_2$ is the only oxygen source in the cell. SE degradation is also evident from the P 2p data. For the cathodes using bare and coated $LiNiO_2$, the intensity of the $P_2S_6^{2-}$ and/or Li_3PO_4 signal is strongly increased after cycling. In addition, the appearance of a new doublet (P $2p_{3/2}$ at 134.1 eV) indicates the formation of oxygenated phosphorus (PO_y) species.[11,41] Quantitative XPS analysis (Figure S9a) confirms that the relative amounts of decomposition products are much lower when using the coated CAM. This is particularly true for the oxygenated sulfur and phosphorus species. Overall, the experimental data clearly demonstrate that the protective surface coating effectively mitigates interfacial degradation, thereby enhancing the battery performance (Figure 3).

Gas analysis via differential electrochemical mass spectrometry (DEMS) also revealed a much weaker m/z = 32 signal (O_2) in the first charge cycle for the cell using the coated CAM (see Figure 4c). Previous studies of layered Ni-rich oxide CAMs in SSB systems attribute the release of oxygen to the destabilization of the lattice structure at high potentials (>4.2 V vs Li+/Li).[13,42,43] The observation here is similar, with the onset potential being ~4.2 V, which corresponds to the unfavorable H2−H3 phase transition. Overall, the DEMS results indicate that the coating is somewhat capable of mitigating the release of lattice oxygen or, in other words, inhibiting the surface phase transformation from layered to spinel/rocksalt and loss of electrochemically active material.[44] This is likely related, to some degree, to the interdiffusion of Nb^{5+} into the $LiNiO_2$, as confirmed by high-resolution STEM

(see Figure S5), which apparently (indirectly) helps to reduce the surface oxygen activity.[19,21,28,45]

The data presented above provide profound evidence for the positive effect of the coating in stabilizing the cathode interface (see Figure 5), which is beneficial to the cell cyclability and

Figure 5. Schematic illustration of the working principle of the $LiNbO_3$ protective surface coating on the $LiNiO_2$ secondary particles.

explains why the coated CAM exhibits better performance, despite the larger absolute changes in unit-cell volume during battery operation.

Having established the optimal coating content, a slurry-cast cathode was prepared from the 0.76 wt % coated $LiNiO_2$ to assess its processability and viability for commercial implementation.[46] Figure 6 summarizes the performance comparison between pelletized and slurry-cast cathodes of similar composition in SSB full cells. It should be noted that the electrode preparation process (wet vs dry processing) did not affect the bulk structure/crystallinity of the CAM and SE (see Figure S10). The slurry-cast cathode contained 1.0 wt % polyisobutylene binder and had a high areal loading of 17.0 mg_{CAM}/cm^2. From the voltage profiles recorded at 45 °C and 0.2C rate (see Figure 6a), it can be seen that the slurry-cast cathode exhibits a lower first-cycle Coulomb efficiency than the pelletized one (Φ_Q = 82 vs 87%) and sacrifices some capacity for cycling stability. Nevertheless, the slurry-cast cathode is capable of delivering higher areal capacities (e.g., 2.4 vs 1.9 mAh/cm^2 in the initial cycle) due to differences in CAM loading and, as mentioned before, has better capacity retention after 100 cycles (84 vs 78%). The improvement in performance/stability is even more significant when increasing the C-rate to 0.5C (see Figure 6b). The pelletized cathode undergoes severe capacity fading from the 160th cycle onward. By contrast, the cell using the slurry-cast cathode exhibits better stability during long-term cycling, still delivering a specific discharge capacity of q_{dis} ≈ 100 mAh/g (equivalent to ~1.7 mAh/cm^2) in the 400th cycle and maintaining a Coulomb efficiency of 99.9%, compared to 99.7% for the pelletized cathode.

The improvement in cyclability is likely due to optimization of the cathode microstructure resulting from the transition from dry to wet processing without other variations.[9,47] To confirm this, the ionic/electronic partial conductivities of the
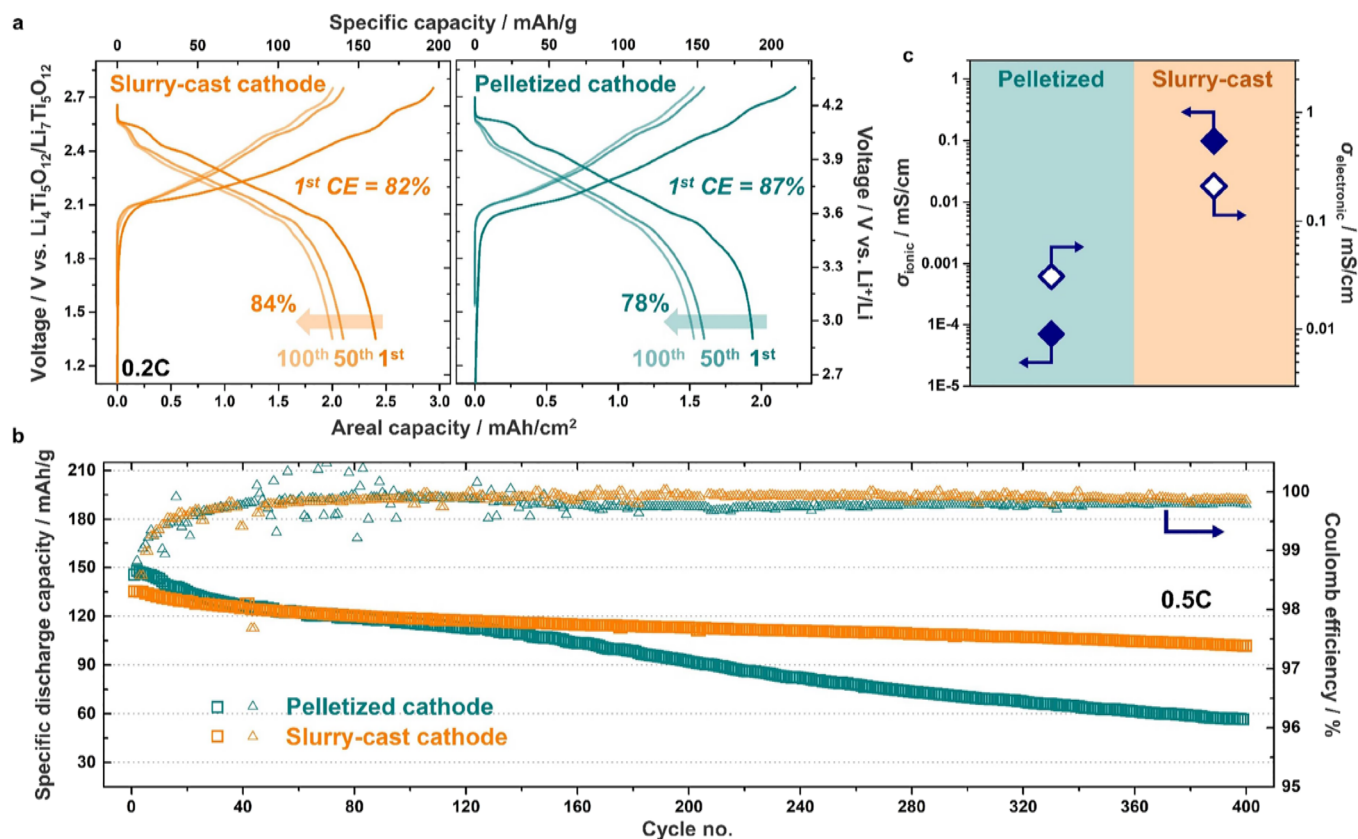
Figure 6. Cyclability of slurry-cast (orange) and pelletized composite cathodes (cyan) using the 0.76 wt % coated $LiNiO_2$ in SSB cells. (a) Voltage profiles for the 1st, 50th, and 100th cycle at 45 °C and 0.2C rate. (b) Long-term cycling performance at 45 °C and 0.5C rate. (c) Mean ionic/electronic partial conductivities.

composite cathodes were determined by room-temperature direct current (DC) polarization measurements under ion/electron-blocking conditions (see Figure S11).[48] As evident from Figure 6c and Table S3, there are major differences in ionic conductivity (σ_{ion}) and electronic conductivity (σ_{elec}) among the samples; especially the σ_{ion} of the slurry-cast cathode is higher by about 3 orders of magnitude than that of the pelletized one. This indicates that wet processing is favorable to achieve highly percolated transport pathways in the electrode (by mitigating particle agglomeration, etc.).[49]

Top-view SEM images of the pelletized and slurry-cast cathodes before and after cycling are shown in Figure 7a. In the pristine state, there are no apparent differences in terms of quality and homogeneity among the electrodes, with the $LiNiO_2$ secondary particles being well embedded in the SE matrix. The slurry-cast cathode retains its original structure (appearance) over hundreds of cycles, and the CAM remains largely intact. In contrast, particle fracture is clearly evident for the pelletized cathode after 200 cycles (at the surface), which becomes more severe with further cycling. After 400 cycles, the secondary particle structure is mostly lost, and only the primary particles (grains) remain. In general, intergranular cracking results from the anisotropic volume changes ("breathing"), interfacial side reactions, and/or heterogeneous SOC distribution during cycling.[50−52] Since the pelletized and slurry-cast cathodes use the same (active) materials, namely, $LiNbO_3$-coated $LiNiO_2$ and Li_6PS_5Cl, we believe that the latter is primarily causing the particle fracture. As discussed above, the pelletized cathode shows inferior ionic/electronic partial conductivities (tortuous transport pathways), which may lead

to nonuniform de/lithiation of the CAM and accumulation of mechanical stress.[51] Note that particle fracture deteriorates with increasing C-rate.[51,52] From the data, it can be concluded that wet processing helps to mitigate some of the problems of SSB composite cathodes while also enabling high loadings.

Considering the poor "wettability" (yield strength) of SEs, previous studies suggest that microcracks formed within CAMs having a loose grain boundary structure primarily exist in the form of voids.[1,7] However, recent studies further point toward (electro)chemically driven interdiffusion reactions and diffusion of mobile SE decomposition species into the secondary particles, which also contributes to performance degradation.[13,53,54] To gain more insights into the interfacial side reactions and their impact on cyclability, XPS measurements were conducted on the pelletized and slurry-cast cathodes after 400 cycles at 45 °C and 0.5C rate (see Figure 7b). In both cases, the S 2p and P 2p spectra show clear signs of interphase formation (i.e., the presence of polysulfide, SO_x, and PO_y species). As expected, the relative amounts of decomposition products from quantitative analysis are lower for the slurry-cast cathode (see Figure S9b). However, the differences are less pronounced compared to those seen for the pelletized cathodes using uncoated or coated $LiNiO_2$ (see Figure S9a). This suggests that diffusion effects play no major role. Instead, mechanical degradation, which strong affects the tortuosity of charge-transport paths, seems to result in the formation of "dead" or less active CAM particles due to contact loss and/or overpotential growth.[35,55]

This is indirectly corroborated by comparative XRD analysis of the slurry-cast and pelletized cathodes before and after
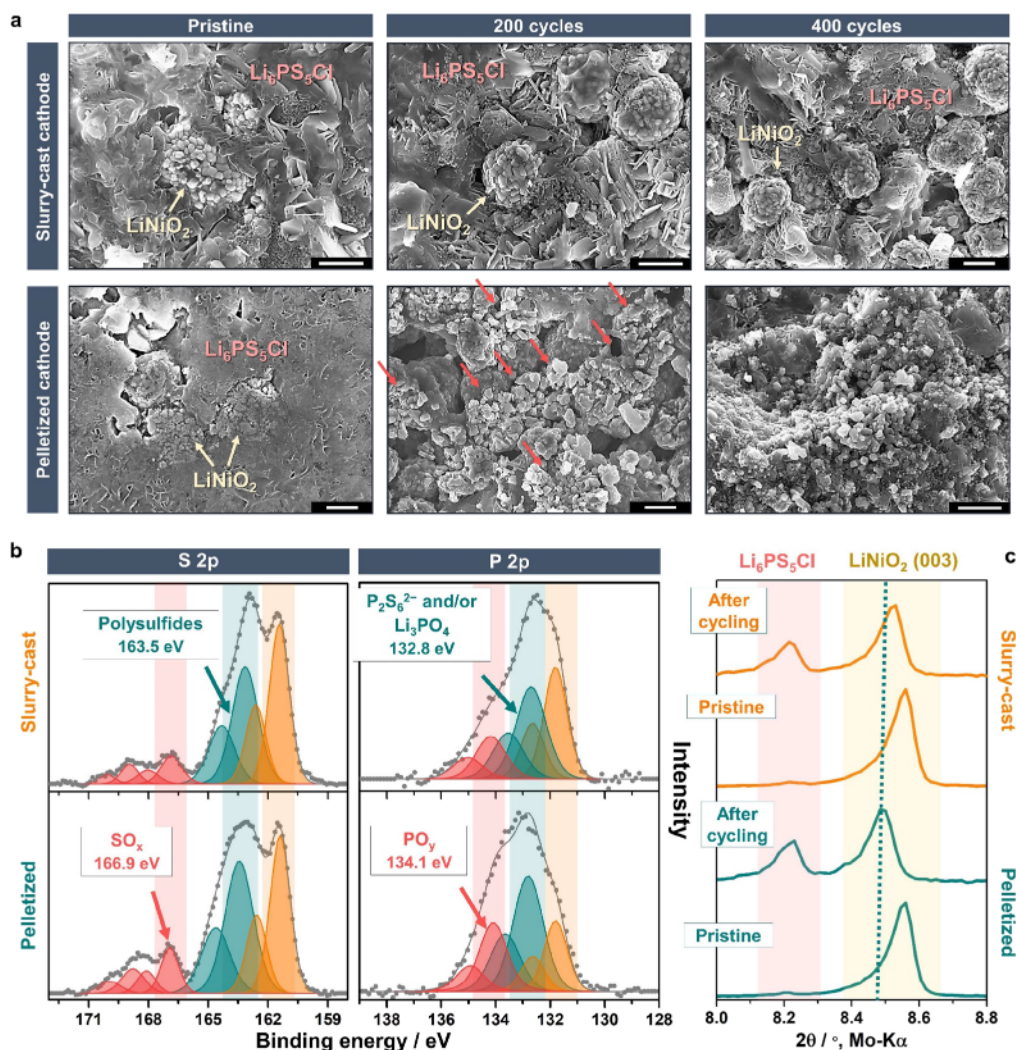
Figure 7. (a) Top-view SEM images of slurry-cast and pelletized composite cathodes using the 0.76 wt % coated $LiNiO_2$ in the pristine state and after 200 and 400 cycles at 45 °C and 0.5C rate. CAM particle fracture is indicated by arrows. (b) Detailed XP spectra showing the S 2p and P 2p core-level regions for the cathodes after 400 cycles. (c) XRD patterns collected from the cathodes before and after cycling in the discharged state.

cycling. As evident from Figure 7c, the 003 reflection of $LiNiO_2$ in the pelletized cathode (discharged state) is shifted to a lower angle after cycling. For the slurry-cast cathode, the reflection also does not fully revert back to its original position. This can be explained by particle fracture leading to electrochemical contact loss during cycling and/or lithium inventory loss due to interfacial side reactions. Regardless, both of these types of degradation are mitigated in the case of the slurry-cast cathode.

Taken together, the above results emphasize that the pelletized cathode (dry processing) experiences significant electrochemomechanical degradation during battery operation. This can be somewhat suppressed in the slurry-cast cathode, resulting in a noticeable enhancement of the cycling stability as wet processing, among others, helps to provide better percolated pathways for the charge carriers. Future studies will focus on gaining a thorough understanding of the effect of micro/nanostructure and cathode composition on the performance.

CONCLUSIONS

This work demonstrates a tailored solid-state battery system that shows high cyclability for a Ni-rich cathode in conjunction with a lithium thiophosphate SE. This is achieved by fabricating a protective coating on the $LiNiO_2$ secondary particle surface and applying wet processing to prepare a slurry-cast electrode. A robust cathode with a high areal loading was obtained, exhibiting good performance in terms of specific capacity, capacity retention, and Coulomb efficiency. Comprehensive characterization, including operando and ex situ/postmortem analyses, revealed that the optimization helps to mitigate side reactions and outgassing and further minimize SOC heterogeneity, which ultimately results in some stabilization of the cathode microstructure and interface. This route should be applicable to other types of composite cathodes, thus facilitating the development of future solid-state battery systems with improved performance.

◼ EXPERIMENTAL SECTION

CAM Preparation. $LiNiO_2$ was synthesized via a solid-state method from hydroxide precursors. $Ni(OH)_2$ (1.0 mol equiv, BASF SE) and $LiOH \cdot H_2O$ (1.01 mol equiv, Sigma-Aldrich) were mixed and calcined at 700 °C for 6 h in an O_2 atmosphere using a heating ramp of 3 °C/min. The as-synthesized material was sieved (45 μm mesh) prior to electrode fabrication. For surface coating, the $LiNiO_2$ particles (6 g) were added to an ethanolic solution containing

lithium and niobium ethoxide in an Ar-glovebox with O_2 and H_2O contents of <0.1 ppm, followed by sonication for 0.5 h. The suspension was then vacuum-dried overnight at room temperature until full evaporation of solvent. The resulting powder was heated at 350 °C for 2 h in an O_2 atmosphere, yielding $LiNbO_3$-coated $LiNiO_2$. Note that samples with different coating contents were prepared by varying the amount of ethoxide precursors in the synthesis.

Structural/Chemical Characterization. SEM images were collected on an LEO-1530 microscope (Carl Zeiss AG) equipped with a field emission source.

A Themis Z (Thermo Fisher Scientific) double-corrected transmission electron microscope was used for TEM characterization. The acceleration voltage was 300 kV. The microscope was equipped with a HAADF detector for STEM acquisition, an EDAX SuperX EDS detector for elemental analysis and mapping, and a Gatan image filter with a K3 camera (Gatan Inc.) for EELS, with an energy resolution of ~1 eV estimated from the fwhm of the zero-loss peak. Specimens (lamellae) for TEM were prepared using a Ga FIB on a STRATA dual-beam system from Thermo Fisher Scientific. A carbon layer was deposited onto the $LiNiO_2$ particle surface prior to ion milling (at 30 kV and final polishing at 2 kV) to avoid damage to the coating.

Powder XRD data were acquired in Debye−Scherrer geometry on a STOE Stadi-P diffractometer with a Mo anode ($\lambda = 0.70926$ Å) and a DECTRIS MYTHEN 1K strip detector. Zero offset and instrumental contribution to peak broadening were determined by measuring a standard reference material, LaB_6 660b. Rietveld refinement was carried out sequentially on the diffraction data using GSAS-II.[56] Samples were packed into Hilgenberg borosilicate glass capillaries with a 0.5 mm inner diameter and 0.01 mm wall thickness.

The operando XRD setup used to monitor the structural evolution of $LiNiO_2$ in LIB coin cells is described elsewhere.[57] The degree of delithiation was estimated from the charge capacity and the mass of active material in the electrode, assuming 100% lithiation [x(Li) = 1] prior to cycling.

A SPECS system with monochromatic Al−Kα radiation ($E = 1486.6$ eV) and a PHOIBOS 150 energy analyzer was used for the XPS data acquisition. The measurements were carried out at a takeoff angle of 45°, with pass energies of 90 and 30 eV for survey and detail scans, respectively. Charging effects were negligible, thus neutralization was not required. For binding-energy calibration, the C 1s peak of adventitious carbon was set to 284.8 eV. Curve fits were performed with the CasaXPS software using a mixed Gaussian−Lorentzian peak function and Shirley-type background. For the P 2p and S 2p core levels, the peak-area ratio and spin−orbit splitting were set to 2:1 and 0.84 eV (P 2p) and 1.18 eV (S 2p), respectively.

The coating content (CAM composition) was determined by ICP-OES using both an iCAP 7600 from Thermo Fisher Scientific and an Optima 4300 DV from PerkinElmer. Specifically, the CAMs were digested in a mixture of HCl and H_2SO_4 at 250 °C for 12 h in Berghof DAB-2 vessels. Mass fractions were obtained from three independent measurements. The range of calibration solutions used did not exceed a decade.

For in situ gas analysis via DEMS, an OmniStar GSD 320 O2 mass spectrometer from Pfeiffer Vacuum GmbH was utilized. The flow of the He carrier gas was controlled by a F-201CV mass flow controller (Bronkhorst). For quantitative analysis, a calibration gas was introduced after the measurements.

Electrode Preparation. Bare (uncoated) or coated $LiNiO_2$, Li_6PS_5Cl (NEI Corp.), and Super C65 (TIMCAL Ltd.) in a weight ratio of 69.3:29.7:1.0 were used in the cathode preparation. For the anode, $LiNiO_2$ was replaced by carbon-coated $Li_4Ti_5O_{12}$ (NEI Corp.). The negative electrode contained 30 wt % $Li_4Ti_5O_{12}$, 65 wt % Li_6PS_5Cl, and 5 wt % Super C65. The powders were placed into a 70 mL zirconia jar with 10 mm diameter zirconia balls and milled at 140 rpm for 30 min by using a planetary ball mill (FRITSCH). The anode and cathode composites were utilized in the assembly of pelletized SSB cells.

For the preparation of cast cathodes, an o-xylene slurry containing 68.6:29.4:1.0:1.0 by weight coated $LiNiO_2$, Li_6PS_5Cl, Super C65, and OPPANOL N 150 polyisobutylene binder (BASF SE) was spread onto Al foil under Ar atmosphere, followed by first natural drying in the glovebox and then vacuum-drying overnight at room temperature.[13]

Cell Assembly and Electrochemical Characterization. SSB cells were assembled in an Ar-glovebox. Their electrochemical behavior was tested using a customized two-electrode setup with stainless steel dies and a 10 mm diameter PEEK sleeve. For pelletized cells, the separator layer was prepared first by pressing 100 mg Li_6PS_5Cl at 62.5 MPa. Next, 12−13 mg of cathode composite (2.4−2.6 mAh/cm^2 assuming q_{dis} = 225 mAh/g) and 65−66 mg of anode composite (4.3−4.4 mAh/cm^2 with q_{th} = 175 mAh/g) in powder form were uniformly spread onto the SE separator (front/back side) and compressed at 440 MPa. For cells with a slurry-cast electrode, the assembly process was the same, with the difference being that the cathode (9 mm in diameter) was punched out and then placed onto the SE separator. The amount of anode composite was calculated based on a negative-to-positive capacity ratio of ~1.74 from pelletized cells.

The electrochemical testing was performed at 45 °C. 1C is defined as 225 mA/g_{CAM}. The cyclability was examined in the voltage window of 1.35−2.75 V vs $Li_4Ti_5O_{12}/Li_7Ti_5O_{12}$ (about 2.9−4.3 V vs Li^+/Li) using a MACCOR battery cycler. EIS data were acquired in the frequency range between 7 MHz and 100 mHz (7 mV AC voltage amplitude) by using a VMP3 potentiostat (BioLogic). Using the same instrument, DC measurements were performed at a constant potential of 300 mV after a 1 h rest period under open circuit voltage conditions.

The SSB cells used for DEMS were assembled in a customized setup described elsewhere.[11,46] They were cycled at 0.05C rate and 45 °C in the potential window of 2.3−3.7 V vs In/InLi (about 2.9−4.3 V vs Li^+/Li) using a VMP3 multichannel potentiostat (BioLogic).

■ AUTHOR INFORMATION

Corresponding Authors

Yuan Ma − *Battery and Electrochemistry Laboratory (BELLA), Institute of Nanotechnology, Karlsruhe Institute of Technology (KIT), 76131 Karlsruhe, Germany;* Present Address: Key Laboratory of Energy Thermal Conversion and Control of Ministry of Education, School of Energy and Environment, Southeast University, Nanjing 211189, China; Email: yuan.ma@seu.edu.cn

Torsten Brezesinski − *Battery and Electrochemistry Laboratory (BELLA), Institute of Nanotechnology, Karlsruhe Institute of Technology (KIT), 76131 Karlsruhe, Germany;* orcid.org/0000-0002-4336-263X; Email: torsten.brezesinski@kit.edu

Authors

Ruizhuo Zhang − *Battery and Electrochemistry Laboratory (BELLA), Institute of Nanotechnology, Karlsruhe Institute of Technology (KIT), 76131 Karlsruhe, Germany*

Yanjiao Ma − *Institute of Nanotechnology, Karlsruhe Institute of Technology (KIT), 76131 Karlsruhe, Germany;* Present

Address: School of Energy and Mechanical Engineering, Jiangsu Key Laboratory of New Power Batteries, Nanjing Normal University, Nanjing 210023, China.

Thomas Diemant − *Helmholtz Institute Ulm (HIU), 89081 Ulm, ◆ermany*

Yushu Tang − *Institute of Nanotechnology and Karlsruhe Nano Micro Facility (KNMFi), Karlsruhe Institute of Technology (KIT), 76131 Karlsruhe, ◆ermany*

Seyedhosein Payandeh − *Battery and Electrochemistry Laboratory (BELLA), Institute of Nanotechnology, Karlsruhe Institute of Technology (KIT), 76131 Karlsruhe, ◆ermany;* ⊙ orcid.org/0000-0003-2828-7106

Damian Goonetilleke − *Battery and Electrochemistry Laboratory (BELLA), Institute of Nanotechnology, Karlsruhe Institute of Technology (KIT), 76131 Karlsruhe, ◆ermany;* Present Address: Umicore, Corporate Research and Development, 2250 Olen, Belgium; ⊙ orcid.org/0000-0003-1033-4787

David Kitsche − *Battery and Electrochemistry Laboratory (BELLA), Institute of Nanotechnology, Karlsruhe Institute of Technology (KIT), 76131 Karlsruhe, ◆ermany*

Xu Liu − *Helmholtz Institute Ulm (HIU), 89081 Ulm, ◆ermany;* ⊙ orcid.org/0000-0003-0532-316X

Jing Lin − *Battery and Electrochemistry Laboratory (BELLA), Institute of Nanotechnology, Karlsruhe Institute of Technology (KIT), 76131 Karlsruhe, ◆ermany*

Aleksandr Kondrakov − *Battery and Electrochemistry Laboratory (BELLA), Institute of Nanotechnology, Karlsruhe Institute of Technology (KIT), 76131 Karlsruhe, ◆ermany; BASF SE, 67056 Ludwigshafen, ◆ermany*

Notes

The authors declare no competing financial interest.

■ REFERENCES

(1) Banerjee, A.; Wang, X.; Fang, C.; Wu, E. A.; Meng, Y. S. Interfaces and Interphases in All-Solid-State Batteries with Inorganic Solid Electrolytes. *Chem. Rev.* 2020, 120, 6878−6933.

(2) Wang, C.; Liang, J.; Zhao, Y.; Zheng, M.; Li, X.; Sun, X. All-Solid-State Lithium Batteries Enabled by Sulfide Electrolytes: From Fundamental Research to Practical Engineering Design. *Energy Environ. Sci.* 2021, 14, 2577−2619.

(3) Chen, R.; Li, Q.; Yu, X.; Chen, L.; Li, H. Approaching Practically Accessible Solid-State Batteries: Stability Issues Related to Solid Electrolytes and Interfaces. *Chem. Rev.* 2020, 120, 6820−6877.

(4) Tan, D. H. S.; Chen, Y.-T.; Yang, H.; Bao, W.; Sreenarayanan, B.; Doux, J.-M.; Li, W.; Lu, B.; Ham, S.-Y.; Sayahpour, B.; Scharf, J.; Wu, E. A.; Deysher, G.; Han, H. E.; Hah, H. J.; Jeong, H.; Lee, J. B.; Chen, Z.; Meng, Y. S. Carbon-Free High-Loading Silicon Anodes Enabled by Sulfide Solid Electrolytes. *Science* 2021, 373, 1494−1499.

(5) Lee, Y.-G.; Fujiki, S.; Jung, C.; Suzuki, N.; Yashiro, N.; Omoda, R.; Ko, D.-S.; Shiratsuchi, T.; Sugimoto, T.; Ryu, S.; Ku, J. H.; Watanabe, T.; Park, Y.; Aihara, Y.; Im, D.; Han, I. T. High-Energy Long-Cycling All-Solid-State Lithium Metal Batteries Enabled by Silver−Carbon Composite Anodes. *Nat. Energy* 2020, 5, 299−308.

(6) Tan, D. H. S.; Banerjee, A.; Chen, Z.; Meng, Y. S. From Nanoscale Interface Characterization to Sustainable Energy Storage Using All-Solid-State Batteries. *Nat. Nanotechnol.* 2020, 15, 170−180.

(7) Minnmann, P.; Strauss, F.; Bielefeld, A.; Ruess, R.; Adelhelm, P.; Burkhardt, S.; Dreyer, S. L.; Trevisanello, E.; Ehrenberg, H.; Brezesinski, T.; Richter, F. H.; Janek, J. Designing Cathodes and Cathode Active Materials for Solid-State Batteries. *Adv. Energy Mater.* 2022, 12, No. 2201425.

(8) Xiao, Y.; Turcheniuk, K.; Narla, A.; Song, A.-Y.; Ren, X.; Magasinski, A.; Jain, A.; Huang, S.; Lee, H.; Yushin, G. Electrolyte Melt Infiltration for Scalable Manufacturing of Inorganic All-Solid-State Lithium-Ion Batteries. *Nat. Mater.* 2021, 20, 984−990.

(9) Zhang, J.; Chen, Z.; Ai, Q.; Terlier, T.; Hao, F.; Liang, Y.; Guo, H.; Lou, J.; Yao, Y. Microstructure Engineering of Solid-State Composite Cathode via Solvent-Assisted Processing. *Joule* 2021, 5, 1845−1859.

(10) Nitta, N.; Wu, F.; Lee, J. T.; Yushin, G. Li-Ion Battery Materials: Present and Future. *Mater. Today* 2015, 18, 252−264.

(11) Ma, Y.; Teo, J. H.; Walther, F.; Ma, Y.; Zhang, R.; Mazilkin, A.; Tang, Y.; Goonetilleke, D.; Janek, J.; Bianchini, M.; Brezesinski, T. Advanced Nanoparticle Coatings for Stabilizing Layered Ni-Rich Oxide Cathodes in Solid-State Batteries. *Adv. Funct. Mater.* 2022, 32, No. 2111829.

(12) Richards, W. D.; Miara, L. J.; Wang, Y.; Kim, J. C.; Ceder, G. Interface Stability in Solid-State Batteries. *Chem. Mater.* 2016, 28, 266−273.

(13) Ma, Y.; Zhang, R.; Tang, Y.; Ma, Y.; Teo, J. H.; Diemant, T.; Goonetilleke, D.; Janek, J.; Bianchini, M.; Kondrakov, A.; Brezesinski, T. Single- to Few-Layer Nanoparticle Cathode Coating for Thiophosphate-Based All-Solid-State Batteries. *ACS Nano* 2022, 16, 18682−18694.

(14) Koerver, R.; Aygün, I.; Leichtweiß, T.; Dietrich, C.; Zhang, W.; Binder, J. O.; Hartmann, P.; Zeier, W. G.; Janek, J. Capacity Fade in Solid-State Batteries: Interphase Formation and Chemomechanical Processes in Nickel-Rich Layered Oxide Cathodes and Lithium Thiophosphate Solid Electrolytes. *Chem. Mater.* 2017, 29, 5574−5582.

(15) Ma, Y.; Teo, J. H.; Kitsche, D.; Diemant, T.; Strauss, F.; Ma, Y.; Goonetilleke, D.; Janek, J.; Bianchini, M.; Brezesinski, T. Cycling Performance and Limitations of LiNiO₂ in Solid-State Batteries. *ACS Energy Lett.* 2021, 6, 3020−3029.

(16) Bianchini, M.; Roca-Ayats, M.; Hartmann, P.; Brezesinski, T.; Janek, J. There and Back Again—The Journey of LiNiO₂ as a Cathode Active Material. *Angew. Chem., Int. Ed.* 2019, 58, 10434−10458.

(17) Wang, L.; Mukherjee, A.; Kuo, C.-Y.; Chakrabarty, S.; Yemini, R.; Dameron, A. A.; DuMont, J. W.; Akella, S. H.; Saha, A.; Taragin, S.; Aviv, H.; Naveh, D.; Sharon, D.; Chan, T.-S.; Lin, H.-J.; Lee, J.-F.; Chen, C.-T.; Liu, B.; Gao, X.; Basu, S.; Hu, Z.; Aurbach, D.; Bruce, P. G.; Noked, M. High-Energy All-Solid-State Lithium Batteries Enabled by Co-Free LiNiO₂ Cathodes with Robust Outside-In Structures. *Nat. Nanotechnol.* 2024, 19, 208.

(18) Park, K. H.; Bai, Q.; Kim, D. H.; Oh, D. Y.; Zhu, Y.; Mo, Y.; Jung, Y. S. Design Strategies, Practical Considerations, and New Solution Processes of Sulfide Solid Electrolytes for All-Solid-State Batteries. *Adv. Energy Mater.* 2018, 8, No. 1800035.

(19) Culver, S. P.; Koerver, R.; Zeier, W. G.; Janek, J. On the Functionality of Coatings for Cathode Active Materials in Thiophosphate-Based All-Solid-State Batteries. *Adv. Energy Mater.* 2019, 9, No. 1900626.

(20) Liu, X.; Zheng, B.; Zhao, J.; Zhao, W.; Liang, Z.; Su, Y.; Xie, C.; Zhou, K.; Xiang, Y.; Zhu, J.; Wang, H.; Zhong, G.; Gong, Z.; Huang, J.; Yang, Y. Electrochemo-Mechanical Effects on Structural Integrity of Ni-Rich Cathodes with Different Microstructures in All Solid-State Batteries. *Adv. Energy Mater.* 2021, 11, No. 2003583.

(21) Yoon, M.; Dong, Y.; Hwang, J.; Sung, J.; Cha, H.; Ahn, K.; Huang, Y.; Kang, S. J.; Li, J.; Cho, J. Reactive Boride Infusion Stabilizes Ni-Rich Cathodes for Lithium-Ion Batteries. *Nat. Energy* **2021**, *6*, 362−371.

(22) Nisar, U.; Muralidharan, N.; Essehli, R.; Amin, R.; Belharouak, I. Valuation of Surface Coatings in High-Energy Density Lithium-Ion Battery Cathode Materials. *Energy Storage Mater.* **2021**, *38*, 309−328.

(23) Kitsche, D.; Tang, Y.; Ma, Y.; Goonetilleke, D.; Sann, J.; Walther, F.; Bianchini, M.; Janek, J.; Brezesinski, T. High Performance All-Solid-State Batteries with a Ni-Rich NCM Cathode Coated by Atomic Layer Deposition and Lithium Thiophosphate Solid Electrolyte. *ACS Appl. Energy Mater.* **2021**, *4*, 7338−7345.

(24) Walther, F.; Strauss, F.; Wu, X.; Mogwitz, B.; Hertle, J.; Sann, J.; Rohnke, M.; Brezesinski, T.; Janek, J. The Working Principle of a $Li_2CO_3/LiNbO_3$ Coating on NCM for Thiophosphate-Based All-Solid-State Batteries. *Chem. Mater.* **2021**, *33*, 2110−2125.

(25) Lin, F.; Markus, I. M.; Doeff, M. M.; Xin, H. L. Chemical and Structural Stability of Lithium-Ion Battery Electrode Materials under Electron Beam. *Sci. Rep.* **2014**, *4*, 5694.

(26) Kim, A.-Y.; Strauss, F.; Bartsch, T.; Teo, J. H.; Hatsukade, T.; Mazilkin, A.; Janek, J.; Hartmann, P.; Brezesinski, T. Stabilizing Effect of a Hybrid Surface Coating on a Ni-Rich NCM Cathode Material in All-Solid-State Batteries. *Chem. Mater.* **2019**, *31*, 9664−9672.

(27) Liu, S.; Liu, Z.; Shen, X.; Li, W.; Gao, Y.; Banis, M. N.; Li, M.; Chen, K.; Zhu, L.; Yu, R.; Wang, Z.; Sun, X.; Lu, G.; Kong, Q.; Bai, X.; Chen, L. Surface Doping to Enhance Structural Integrity and Performance of Li-Rich Layered Oxide. *Adv. Energy Mater.* **2018**, *8*, No. 1802105.

(28) Nunes, B. N.; van den Bergh, W.; Strauss, F.; Kondrakov, A.; Janek, J.; Brezesinski, T. The Role of Niobium in Layered Oxide Cathodes for Conventional Lithium-Ion and Solid-State Batteries. *Inorg. Chem. Front.* **2023**, *10*, 7126−7145.

(29) Asenbauer, J.; Varzi, A.; Passerini, S.; Bresser, D. Revisiting the Energy Efficiency and (Potential) Full-Cell Performance of Lithium-Ion Batteries Employing Conversion/Alloying-Type Negative Electrodes. *J. Power Sources* **2020**, *473*, No. 228583.

(30) Ma, Y.; Ma, Y.; Dreyer, S. L.; Wang, Q.; Wang, K.; Goonetilleke, D.; Omar, A.; Mikhailova, D.; Hahn, H.; Breitung, B.; Brezesinski, T. High-Entropy Metal−Organic Frameworks for Highly Reversible Sodium Storage. *Adv. Mater.* **2021**, *33*, No. 2101342.

(31) Mücke, R.; Finsterbusch, M.; Kaghazchi, P.; Fattakhova-Rohlfing, D.; Guillon, O. Modelling Electro-Chemical Induced Stresses in All-Solid-State Batteries: Anisotropy Effects in Cathodes and Cell Design Optimisation. *J. Power Sources* **2021**, *489*, No. 229430.

(32) Goonetilleke, D.; Sharma, N.; Pang, W. K.; Peterson, V. K.; Petibon, R.; Li, J.; Dahn, J. R. Structural Evolution and High-Voltage Structural Stability of $Li(Ni_xMn_yCo_z)O_2$ Electrodes. *Chem. Mater.* **2019**, *31*, 376−386.

(33) Koerver, R.; Zhang, W.; de Biasi, L.; Schweidler, S.; Kondrakov, A. O.; Kolling, S.; Brezesinski, T.; Hartmann, P.; Zeier, W. G.; Janek, J. Chemo-Mechanical Expansion of Lithium Electrode Materials - On the Route to Mechanically Optimized All-Solid-State Batteries. *Energy Environ. Sci.* **2018**, *11*, 2142−2158.

(34) Goonetilleke, D.; Riewald, F.; Kondrakov, A. O.; Janek, J.; Brezesinski, T.; Bianchini, M. Alleviating Anisotropic Volume Variation at Comparable Li Utilization during Cycling of Ni-Rich, Co-Free Layered Oxide Cathode Materials. *J. Phys. Chem. C* **2022**, *126*, 16952−16964.

(35) Jung, S. H.; Kim, U.; Kim, J.; Jun, S.; Yoon, C. S.; Jung, Y. S.; Sun, Y. Ni-Rich Layered Cathode Materials with Electrochemo-Mechanically Compliant Microstructures for All-Solid-State Li Batteries. *Adv. Energy Mater.* **2020**, *10*, No. 1903360.

(36) Shi, T.; Zhang, Y.-Q.; Tu, Q.; Wang, Y.; Scott, M. C.; Ceder, G. Characterization of Mechanical Degradation in an All-Solid-State Battery Cathode. *J. Mater. Chem. A* **2020**, *8*, 17399−17404.

(37) Zhang, R.; Ma, Y.; Tang, Y.; Goonetilleke, D.; Diemant, T.; Janek, J.; Kondrakov, A.; Brezesinski, T. Conformal Li_2HfO_3/HfO_2 Nanoparticle Coatings on Layered Ni-Rich Oxide Cathodes for Stabilizing Interfaces in All-Solid-State Batteries. *Chem. Mater.* **2023**, *35*, 6835−6844.

(38) Wang, B.; Liu, J.; Sun, Q.; Li, R.; Sham, T.-K.; Sun, X. Atomic Layer Deposition of Lithium Phosphates as Solid-State Electrolytes for All-Solid-State Microbatteries. *Nanotechnology* **2014**, *25*, No. 504007.

(39) Park, S. W.; Oh, G.; Park, J. W.; Ha, Y.-C.; Lee, S.-M.; Yoon, S. Y.; Kim, B. G. Graphitic Hollow Nanocarbon as a Promising Conducting Agent for Solid-State Lithium Batteries. *Small* **2019**, *15*, No. 1900235.

(40) Wang, L.; Sun, X.; Ma, J.; Chen, B.; Li, C.; Li, J.; Chang, L.; Yu, X.; Chan, T.-S; Hu, Z.; Noked, M.; Cui, G. Bidirectionally Compatible Buffering Layer Enables Highly Stable and Conductive Interface for 4.5 V Sulfide-Based All-Solid-State Lithium Batteries. *Adv. Energy Mater.* **2021**, *11*, No. 2100881.

(41) Auvergniot, J.; Cassel, A.; Ledeuil, J.-B.; Viallet, V.; Seznec, V.; Dedryvère, R. Interface Stability of Argyrodite Li_6PS_5Cl toward $LiCoO_2$, $LiNi_{1/3}Co_{1/3}Mn_{1/3}O_2$, and $LiMn_2O_4$ in Bulk All-Solid-State Batteries. *Chem. Mater.* **2017**, *29*, 3883−3890.

(42) Jung, R.; Metzger, M.; Maglia, F.; Stinner, C.; Gasteiger, H. A. Oxygen Release and Its Effect on the Cycling Stability of $LiNi_xMn_yCo_zO_2$ (NMC) Cathode Materials for Li-Ion Batteries. *J. Electrochem. Soc.* **2017**, *164*, A1361−A1377.

(43) Jung, R.; Strobl, P.; Maglia, F.; Stinner, C.; Gasteiger, H. A. Temperature Dependence of Oxygen Release from $Li-Ni_{0.6}Mn_{0.2}Co_{0.2}O_2$ (NMC622) Cathode Materials for Li-Ion Batteries. *J. Electrochem. Soc.* **2018**, *165*, A2869−A2879.

(44) Kobayashi, S.; Watanabe, H.; Kato, T.; Mizuno, F.; Kuwabara, A. Atomic-Scale Observations of Oxygen Release Degradation in Sulfide-Based All-Solid-State Batteries with Layered Oxide Cathodes. *ACS Appl. Mater. Interfaces* **2022**, *14*, 39459−39466.

(45) Wu, H.; Zhou, X.; Yang, C.; Xu, D.; Zhu, Y.-H.; Zhou, T.; Xin, S.; You, Y. Concentration-Gradient Nb-Doping in a Single-Crystal $LiNi_{0.83}Co_{0.12}Mn_{0.05}O_2$ Cathode for High-Rate and Long-Cycle Lithium-Ion Batteries. *ACS Appl. Mater. Interfaces* **2023**, *15*, 18828−18835.

(46) Teo, J. H.; Strauss, F.; Tripković, Đ.; Schweidler, S.; Ma, Y.; Bianchini, M.; Janek, J.; Brezesinski, T. Design-of-Experiments-Guided Optimization of Slurry-Cast Cathodes for Solid-State Batteries. *Cell Rep. Phys. Sci.* **2021**, *2*, No. 100465.

(47) Teo, J. H.; Strauss, F.; Walther, F.; Ma, Y.; Payandeh, S.; Scherer, T.; Bianchini, M.; Janek, J.; Brezesinski, T. The Interplay between (Electro)Chemical and (Chemo)Mechanical Effects in the Cycling Performance of Thiophosphate-Based Solid-State Batteries. *Mater. Futures* **2022**, *1*, No. 015102.

(48) Strauss, F.; Bartsch, T.; de Biasi, L.; Kim, A.-Y.; Janek, J.; Hartmann, P.; Brezesinski, T. Impact of Cathode Material Particle Size on the Capacity of Bulk-Type All-Solid-State Batteries. *ACS Energy Lett.* **2018**, *3*, 992−996.

(49) Jiang, W.; Zhu, X.; Huang, R.; Zhao, S.; Fan, X.; Ling, M.; Liang, C.; Wang, L. Revealing the Design Principles of Ni-Rich Cathodes for All-Solid-State Batteries. *Adv. Energy Mater.* **2022**, *12*, No. 2103473.

(50) Han, D.; Weng, J.; Zhang, X.; Tong, Q.; Zhu, M. Review—Revealing the Intercrystalline Cracking Mechanism of NCM and Some Regulating Strategies. *J. Electrochem. Soc.* **2022**, *169*, No. 040512.

(51) Xia, S.; Mu, L.; Xu, Z.; Wang, J.; Wei, C.; Liu, L.; Pianetta, P.; Zhao, K.; Yu, X.; Lin, F.; Liu, Y. Chemomechanical Interplay of Layered Cathode Materials Undergoing Fast Charging in Lithium Batteries. *Nano Energy* **2018**, *53*, 753−762.

(52) Li, J.; Huang, J.; Li, H.; Kong, X.; Li, X.; Zhao, J. Insight into the Redox Reaction Heterogeneity within Secondary Particles of Nickel-Rich Layered Cathode Materials. *ACS Appl. Mater. Interfaces* **2021**, *13*, 27074−27084.

(53) Zhang, R.; Strauss, F.; Jiang, L.; Casalena, L.; Li, L.; Janek, J.; Kondrakov, A.; Brezesinski, T. Transition-Metal Interdiffusion and Solid Electrolyte Poisoning in All-Solid-State Batteries Revealed by Cryo-TEM. *Chem. Commun.* **2023**, *59*, 4600−4603.

(54) Lee, K.-J.; Byeon, Y.-W.; Lee, H.-J.; Lee, Y.; Park, S.; Kim, H.-R.; Kim, H.-K.; Oh, S. J.; Ahn, J.-P. Revealing Crack-Healing Mechanism of NCM Composite Cathode for Sustainable Cyclability of Sulfide-Based Solid-State Batteries. *Energy Storage Mater.* **2023**, *57*, 326−333.

(55) Han, Y.; Jung, S. H.; Kwak, H.; Jun, S.; Kwak, H. H.; Lee, J. H.; Hong, S.; Jung, Y. S. Single- or Poly-Crystalline Ni-Rich Layered Cathode, Sulfide or Halide Solid Electrolyte: Which Will Be the Winners for All-Solid-State Batteries? *Adv. Energy Mater.* **2021**, *11*, No. 2100126.

(56) Toby, B. H.; Von Dreele, R. B. ◖*SAS-II*: The Genesis of a Modern Open-Source All Purpose Crystallography Software Package. *J. Appl. Crystallogr.* **2013**, *46*, 544−549.

(57) de Biasi, L.; Schiele, A.; Roca-Ayats, M.; Garcia, G.; Brezesinski, T.; Hartmann, P.; Janek, J. Phase Transformation Behavior and Stability of $LiNiO_2$ Cathode Material for Li-Ion Batteries Obtained from In Situ Gas Analysis and Operando X-Ray Diffraction. *ChemSusChem* **2019**, *12*, 2240−2250.